Phase-field modelling of a miscible system in spinning droplet tensiometer

Anatoliy Vorobev

Energy Technology Research Group, Faculty of Engineering and the Environment, University of Southampton, Southampton, SO17 1BJ, UK; Institute of Continuous Media Mechanics UB RAS, Perm, 614013, Russia

Andrea Boghi

School of Energy, Environment and Agrifood, Cranfield University, Cranfield, MK43 0AL, UK

Abstract

The spinning drop tensiometry is used for measurements of surface tension coefficients, especially, when interfaces are characterised by low and ultra-low interfacial stresses. A droplet of lighter liquid is introduced into a rotating capillary that was initially saturated with another heavier liquid. The tube is subject to axial rotation that results in droplet's elongation along the tube's axis. The equilibrium shape of the droplet is used to determine the surface tension coefficient. In this work, the evolution of a slowly miscible droplet introduced into a spinning capillary is investigated. This technique is frequently employed for studies of the dynamics of miscible systems, even despite the fact that a strict equilibrium is never achieved in a mixture of fully miscible liquids. The numerical modelling of a miscible droplet is fulfilled on the basis of the phase-field (Cahn-Hilliard) approach. The numerical results are compared against the experimental data pursuing two objectives: (i) to verify the use of the phase-field approach as a consistent physics-based approach capable of accurate tracking of the short- and long-term evolution of miscible systems, and (ii) to estimate the values of the phenomenological parameters introduced within the phase-field approach, so making this approach a practical tool for modelling of thermohydrodynamic changes in miscible systems within various configurations.

Keywords: miscible interface, phase-field approach, Cahn-Hilliard-Navier-Stokes equations, spinning drop tensiometer

1. Introduction

In a tube with two closed ends filled with two immiscible liquids and then rotated about its axis, the centrifugal force separates the liquids so that a lighter one tends to occupy the inner part of the tube, while the heavier liquid occupies the outer part. The surface tension associated with the liquid/liquid interface aims to restore the spherical shape of the droplet. In a state of mechanical equilibrium, the droplet has an ellipsoidal shape defined by the balance of the centrifugal and surface tension forces. The equilibrium shape of the droplet is used to determine the value of the surface tension coefficient for the liquid/liquid interface.

Vonnegut [1] derived a simple formula to relate the surface tension coefficient to the droplet's dimensions. His formula assumes that the droplet is strongly elongated so it can be roughly represented as a cylinder of radius $a_r R$ and length $2a_z R$ (here R is the tube's radius, and a_r and a_z are the non-dimensional radial and axial dimensions of the droplet), with two hemispherical ends. The surface tension coefficient is then given by,

$$\sigma = \frac{1}{4}(\rho_1 - \rho_2)\Omega^2(a_r R)^3, \tag{1}$$

where ρ_1 and ρ_2 are the densities of two liquids in a mixture, and Ω is the angular velocity. Expression (1) is valid for sufficiently elongated droplets, when $a_z > 2a_r$, which is generally true for higher speeds of the tube's rotation.

This idea was employed to build a number of spinning drop apparatuses, see e.g [2, 3]. Further improvements to the design of a spinning drop tensiometer were suggested in a number of other studies. For instance, the case of lower rotation speeds, when buoyancy ef-

Email addresses: A.Vorobev@soton.ac.uk (Anatoliy Vorobev), a.boghi@cranfield.ac.uk (Andrea Boghi)

fects may become essential are examined in [4, 5, 6]. Inertial oscillations of the liquid/liquid interfaces were studied in [5]. Criteria to avoid the adhesion of a droplet to the tube walls were provided by Princen et al. [7], and, on the contrary, the spinning droplet technique was modified for measurements of the contact angles at the liquid/liquid/solid contact in another work by Princen and Vaidya [8]. In [9], a tube of square cross section was used, which permitted interpretation of the experimental data without knowledge of the refraction index of a denser liquid (this was normally needed to take into account the apparent magnification of the droplet).

The main advantages of the spinning drop method are as follows, (i) the force that determines the droplet's shape, i.e. the centrifugal force, can be varied at will, in contrast to the techniques based on the action of the gravity force (pendant drop, sessile drop), (ii) the technique can be successfully employed for measurements of ultra-small values of interfacial stress, and (iii) the shape of the droplet is stable under 'normal' experimental conditions. There are several shortcomings as well. The main difficulty was found to be a sensitivity of a mechanical equilibrium of the droplet to e.g. alignment of the spinning tube, warming up of the apparatus, etc. For instance, Chan et al. [10] reported that the measured surface tension coefficient was a function of the rotation rate in their experiments. The reason of such dependence remained unexplained, with likely explanation that the liquid/liquid system did not reach the equilibrium state.

In the current work we deal with the surface tension introduced for an interface between two miscible liquids [11]. The surface tension stems from the difference in intermolecular interactions in different liquids at different sides of the interface. For a slowly miscible interface, such a difference in intermolecular forces would still exist for prolong time periods, resulting in e.g. a spherical shape of a honey droplet that is immersed in tea (despite the fact that honey and water are fully miscible). The need to introduce the surface tension for miscible interfaces was first pointed out by Korteweg [12] and van der Waals [13], and later by Zeldovich [14], Joseph [15] and others. The interfacial stresses for miscible systems are low and the interfacial diffusion makes the surface tension process-dependent. Nevertheless, the existence of the surface tension at miscible interfaces was confirmed in a number of experiments [16, 17, 18, 19, 20, 21]. Such measurements were possible, as the changes in the surface tension were slower than the time needed for the measurements.

The use of the spinning drop tensiometry for measurements of the surface tension between two miscible liquids was first reported in [22, 23]. Later, similar measurements were undertaken by Pojman's group [19, 20], who found that the Vonnegut formula holds for long time periods after the liquids reach a thermal equilibrium. The time-changes in the surface tension upon dissolution of the droplet were reported. It was also found that the surface tension was independent of the rotation rate for the speeds over 6000 rpm, and it was independent of the initial droplet volume. It was also observed, that the droplet's interface remains sharp for the entire duration of the dissolution process.

A few numerical simulations of the droplet evolution in a spinning drop tensiometer were carried out. Hu and Joseph [24] studied the evolution of an immiscible system using a finite element formulation to solve the Navier-Stokes equations and a mixed Lagrangian and Eulerian technique to describe the interface motion. They found that the rate of the droplet's evolution depends on the surface tension, the viscosities of both liquids, and on the final equilibrium radius of a droplet. The evolution of a mixture of two miscible liquids within the spinning tube was undertaken in [25], whose work included the account of the interfacial tension, defined by the Korteweg stress. The interfacial diffusion was however defined through the standard Fick's law, which made impossible to reproduce the long-term evolution of the droplet.

The system of consistent equations for the thermo- and hydrodynamic evolution of a two-phase mixture of miscible liquids was derived by Lowengrub and Truskinovsky [26]. This system takes into account the effect of the Korteweg stresses in the momentum equation and considers the mass flux as a linear function of the chemical potential gradient instead of the concentration gradient. The full system of equations is compressible (due to dependence of mixture density on concentration) and its direct numerical solution is hardly feasible. The Boussinesq approximation of the Cahn-Hilliard-Navier-Stokes equations was derived in [27]. The equations in the Boussinesq approximation for a heterogeneous mixture of miscible liquids are similar to the equations previously used by e.g. Jacqmin [28] for modelling of the evolution of immiscible interfaces. The difference is in the barodiffusion term that appears in the expression for the chemical potential. The Boussinesq approximation of the Cahn-Hilliard-Navier-Stokes equations is used for the numerical simulations in the current work.

It should be also noted that the phase-field approach introduces the new phenomenological parameters (e.g. the capillary constant is used instead of the surface tension coefficient). The values of these parameters are currently unknown. There are only some estimates of

the capillary constant in e.g. [29, 30]. The lack of knowledge of these new parameters hinders the wider usage of the phase-field method. In order to estimate the values of the introduced phenomenological parameters, and so to make the phase-field approach a practical tool for consideration of miscible multiphase systems in other configurations, the numerical results to be obtained in the current study are compared with the existent experimental data [22, 19, 20]. Instances when mixing of two liquids is essential are ubiquitous in nature and industry, including the processes of enhanced oil recovery (miscible displacement), aquifer remediation, chemical extraction of vegetable oils, etc. [31, 32, 11]. In general, mixing of liquid/liquid and gas/liquid chemicals is required prior to chemical reactions can occur, and hence accurate description of the mixing is needed for modelling of almost every chemical engineering process.

2. Problem statement

We consider the evolution of two liquids that saturates a capillary tube with circular cross-section of radius R. The tube rotates around its axis with the angular velocity Ω. We assume that the liquid/liquid mixture is isothermal.

The density of the liquid/liquid mixture is a function of concentration, which is defined by the following simple linearised relation,

$$\bar{\rho} = \rho_1(1 + \phi\bar{C}),\ \phi \equiv \frac{\rho_2 - \rho_1}{\rho_2}. \tag{2}$$

This expression is valid for small density contrasts, ϕ, which is generally true for all liquid/liquid mixtures. Concentration $\bar{C}$ is defined as the mass fraction of one of the components in the mixture.

Within the phase-field approach, one set of equations is used to define the whole multiphase system (both liquids and the interface). To derive the governing equations for the system evolution, the specific free energy function, f, is defined as the function of concentration and concentration gradient [33],

$$f = f_0(\bar{C}) + \frac{\epsilon}{2}\left|\nabla\bar{C}\right|^2. \tag{3}$$

The second term in the above expression (3) takes into account the surface tension effects. The amplitude of this term is defined by the capillary coefficient ϵ, which is generally small so the capillary addition to the free energy function is only important at the places of large concentration gradients, i.e. at interfaces.

The classical part of the free energy, f_0, defines the possible states of the binary mixture. We wish to examine the dissolution of a liquid droplet in another liquid, when an initially heterogeneous system transforms into a homogeneous state. The simplest free energy function that permits such transition, is given by the Landau expression [34]

$$f_0 = a(\bar{C} - C_{cr})^2 + b(\bar{C} - C_{cr})^4, \tag{4}$$

where C_{cr} is the concentration in the critical point, and a and b are the phenomenological parameters. This expression defines the binary systems with the upper critical (consolute) point: a binary system is homogeneous if the mixture temperature is above the critical point and heterogeneous if the mixture temperature is below the critical temperature. The Landau function was initially written for the system near the thermodynamic critical point. The first parameter a is proportional to $(T - T_{cr})$, i.e. positive above the critical point, and negative below the critical point. The second parameter b is always positive.

For convenience, in the following expression the concentration and density fields are redefined as follows $(\bar{C} - C_{cr}) \to C$ and $(\bar{\rho} - \rho_{cr}) \to \rho$.

The governing equations for the mixture of two incompressible liquids are called the Cahn-Hilliard-Navier-Stokes equations. The Boussinesq approximation of the full equations written in the non-dimensional form is [27],

$$\frac{\partial\vec{u}}{\partial t} + (\vec{u}\cdot\nabla)\vec{u} = -\nabla\Pi + \frac{1}{\mathrm{Re}}\nabla^2\vec{u} - C\nabla\mu - 2r\mathrm{Gr}C\vec{e}_r, \tag{5}$$

$$\frac{\partial C}{\partial t} + (\vec{u}\cdot\nabla)C = \frac{1}{\mathrm{Pe}}\nabla^2\mu, \tag{6}$$

$$\nabla\cdot\vec{u} = 0, \tag{7}$$

$$\mu = -\frac{\mathrm{Gr}}{2}r^2 + \mu_0 - Ca\nabla^2 C, \quad \mu_0 = \frac{df_0}{dC}. \tag{8}$$

The conventional notations are used for the variables, namely, $\vec{u}$, Π, and μ are the fields of velocity, pressure, and chemical potential, respectively. The problem is solved in cylindrical coordinates with the radial and axial coordinates denoted by r and z. In equation (5), the centrifugal force is taken into account, while the gravity and Coriolis forces are neglected, which is possible at sufficiently high rotation rates (similar assumption were made e.g. in [24, 25]).[1] Here, $\vec{e}_r$ is the unit vector in the radial direction.

[1] At lower rotation rates, the droplet is displaced away from the axis due to combination of Coriolis and buoyancy forces (see e.g. [6]), which is not studied in our work.

To non-dimensionalize these equations the following scales of length L_*, time τ_*, velocity v_*, pressure p_*, and chemical potential μ_* were chosen

$$L_* = R,\ \tau_* = \frac{R}{v_*},\ v_* = b^{1/2},\ p_* = \rho_1 b,\ \mu_* = b. \quad (9)$$

Here, ρ_1 is the density of liquid 1. The non-dimensional parameters entering the governing equations include the Peclet number

$$\mathrm{Pe} = \frac{\rho_* R}{\alpha b^{1/2}}, \quad (10)$$

where α is the mobility coefficient; the capillary number,[2]

$$\mathrm{Ca} = \frac{\epsilon}{bR^2}; \quad (11)$$

the Reynolds number,

$$\mathrm{Re} = \frac{\rho_* b^{1/2} R}{\eta_1}, \quad (12)$$

with η_1 being the viscosity of liquid 1[3]; and the rotational analogue of the Grashof number,

$$\mathrm{Gr} = \phi \frac{(\Omega R)^2}{b}. \quad (13)$$

The thermodynamic state of the binary mixture is defined by one parameter $A = a/b$.

We need to notice that we use the standard names for some of the above non-dimensional parameters. In the governing equations, these parameters would appear in front of the corresponding terms, and hence, would determine the similar effects. For instance, the Prandtl number defines the role of diffusion, the Reynolds number determines the strength of the viscous force, and the Grashof number is the strength of the centrifugal force. These parameters are though introduced through the phenomenological parameters of the phase-field approach.

The classical part of the chemical potential μ is denoted by μ_0. For the Landau free energy, this part is

$$\mu_0 = 2AC + 4C^3. \quad (14)$$

[2]This parameter is sometimes called the Cahn number. We call it the capillary number, since it is proportional to the capillary constant, and defines the strength of the capillary effects. It should be noted though that this parameter is different from the classical capillary number, $\eta_1 v_*/\sigma_*$, introduced within a convectional Laplacian approach.

[3]We assume that the viscosity coefficients of the liquids in the mixture are different, but these difference is not large, and only the leading term of the viscous force is needed in equation (5)[27].

In this work, a different expression for the numerical simulations is however used, namely,

$$\mu_0 = \frac{3}{4} \ln\left(\frac{1/2 + C}{1/2 - C}\right) - (3 - 2A)C. \quad (15)$$

The latter formula coincides with the Landau expression (14) near the critical point, $C = 0$. Formula (15) is more convenient for description of the states far from the critical point, when $|C| \approx 1/2$. It is known that the expression based on the Landau free energy function (14) allows overshooting of the concentration levels $1/2$ and $-1/2$ (these two levels correspond to pure components of the binary mixture). Such an overshooting is deemed permissible, and it is present in all works that are based on the phase-field approach, but still it is not desirable. For modified function (15), the concentration field remains bounded within the range $-1/2..1/2$.

If the speed of rotations is sufficiently high, all experimental pictures [19, 20] possess the axial symmetry, which is also assumed for the numerical simulations of the current work. The droplet is located in the middle of the tube. Both ends of the tube are equivalent. This allows us to consider only the quarter of the droplet, limiting the computational domain by the lines $r = 0$ and $r = 1$, and $z = 0$ and $z = H$ (see Fig. 1). It is assumed that the droplet is considerably smaller than the length of the tube, and the tube's length $2H$ is taken sufficiently high to exclude the influence of the tube's ends on the numerical results.

The boundary conditions imposed on the solutions of the governing equations are as follows. At the tube's wall, the no-slip boundary condition is imposed for the velocity field and no diffusive flux through the wall is set for the field of chemical potential. In addition, we need to specify the wetting conditions at the wall. For simplicity (and because our current focus is not on the droplet/wall interactions), we assume that the molecules of both liquids interact with the wall equally, and hence, the additional boundary condition can be written in a simplistic form: zero normal component of the concentration gradient at the wall, which signifies that the contact line is orthogonal to the wall. Thus, at $r = 1$,

$$u_r = 0,\ u_z = 0,\ \frac{\partial \mu}{\partial r} = 0,\ \frac{\partial C}{\partial r} = 0. \quad (16)$$

At the centreline, $r = 0$, the symmetry boundary conditions are imposed,

$$u_r = 0,\ \frac{\partial u_z}{\partial r} = 0,\ \frac{\partial \mu}{\partial r} = 0,\ \frac{\partial C}{\partial r} = 0. \quad (17)$$

We consider only a quarter of the droplet. At the bottom of the computational domain, $z = 0$, the imposed

boundary conditions are

$$\frac{\partial u_r}{\partial z} = 0,\ u_z = 0,\ \frac{\partial \mu}{\partial z} = 0,\ \frac{\partial C}{\partial z} = 0. \tag{18}$$

At the upper side, $z = H$, we impose the free-stress boundary conditions,

$$\frac{\partial u_r}{\partial z} = 0,\ u_z = 0,\ \frac{\partial \mu}{\partial z} = 0,\ \frac{\partial C}{\partial z} = 0. \tag{19}$$

For numerical solution, the equations were re-written in terms of the vorticity (ω) and streamfunction (ψ), which are introduced by the following formulae,

$$u_r = -\frac{1}{r}\frac{\partial \psi}{\partial z},\ u_z = \frac{1}{r}\frac{\partial \psi}{\partial r},\ \omega = \frac{\partial u_r}{\partial z} - \frac{\partial u_z}{\partial r}. \tag{20}$$

Here u_r and u_z are the radial and axial components of the velocity.

The numerical problem was solved by using the method of finite differences. We used the uniform grid, and the finite difference formulae of the second order. The grid was sufficiently fine to include several points within the interface (in analogy with [35, 36]).

It is known that the interface thickness is defined by the parameters Ca and A. Thus, for a mixture with thermodynamics defined by the Landau expression (4), a flat interface in the absence of the external fields is defined by the following concentration profile,

$$C_0(x) = \sqrt{-\frac{A}{2}}\tanh\left(\frac{x}{\delta_0}\right),\ \delta_0 = \sqrt{-\frac{\mathrm{Ca}}{A}}, \tag{21}$$

where x is the coordinate across the interface and δ_0 is the interface thickness. These formulae are needed to adapt the size of the computational grid when Ca and A are changed.

Within the phase-field approach, the surface tension can be defined as

$$\sigma_{\mathrm{CH}} = \mathrm{Ca}\int_{-\infty}^{+\infty}\left(\frac{dC}{dx}\right)^2 dx. \tag{22}$$

This gives the following expression for a flat interface,

$$\sigma_0 = \frac{2}{3}A^2\sqrt{-A\mathrm{Ca}}, \tag{23}$$

i.e. the surface tension is proportional to $\sqrt{\mathrm{Ca}}$, which would be useful for the analysis of the numerical results.

Each simulation was initialised by assuming that a 'fresh' spherical droplet is introduced into a pure solvent,

$$C_{in}(r,z) = \frac{1}{2}\tanh\left(\frac{\sqrt{r^2+z^2}-r_0}{\delta_{in}}\right), \tag{24}$$

where r_0 is the initial radius of the droplet, and the concentrations $\pm\frac{1}{2}$ represent pure solute and solvent. The initial interface thickness, δ_{in}, was taken to be equal 4 steps of the computational mesh.[4] The tube's rotations are switched on at the start of the numerical run. The half-length of the tube is $H = 3$ for all results presented below. The parameter A is taken to be -0.5.

3. Numerical results

The time evolution of the droplet is shown in figure 1 through the set of snapshots. During the entire evolution the interface remains sharp which agrees with the experimental observations [22, 19, 20]. In the first instances, the droplet elongates along the tube's axis, reaching the quasi-equilibrium state when the capillary and centrifugal forces are nearly balanced. In contrast to an immiscible system, the complete equilibration cannot be achieved. The droplet is slowly dissolving due to interfacial mass transfer, and this process results in constant changes of the quasi-equilibrium shape. At the end of the dissolution, when the droplet becomes relatively small, the role of the capillary force increases, and the droplet becomes nearly spherical.

The evolution of the droplet is accompanied by the hydrodynamic flow that is driven by the non-homogeneities in the density field. The flow consists of two vorticies (one vortex in the modelled part of the domain, and another vortex is in the second, not-shown, half of the tube).

Figure 1 also depicts the isolines of the chemical potential. The intensity of the interfacial diffusion is determined by the gradients of the chemical potential: the diffusion should be stronger at the droplet's 'equator', from where the molecules of the solute are transported by the flow along the droplet's surface towards the droplet's ends, and then into the other parts of the tube. These results, including appearance of the cloudy regions near the droplet's ends, are is in agreement with the experimental pictures [22].

Figure 2 depicts the results of the numerical simulations of the droplet's time evolution obtained for the

[4] In [37, 38], the influence of the interface thickness on the stability of a phase boundary has been studied. It has been found that if the interface thickness is smaller than the thickness that corresponds to the thermodynamic equilibrium value δ_0 (21), then the thickness of the transition zone quickly adjusts to the thermodynamic equilibrium value, i.e. there is no disintegration of the phase boundary. If however the interface thickness is greater than δ_0, then the dynamics of the interface is more complex. In the current work, we always assume that at the initial point the interface thickness is nearly zero that should correspond to the first contact of two liquids.

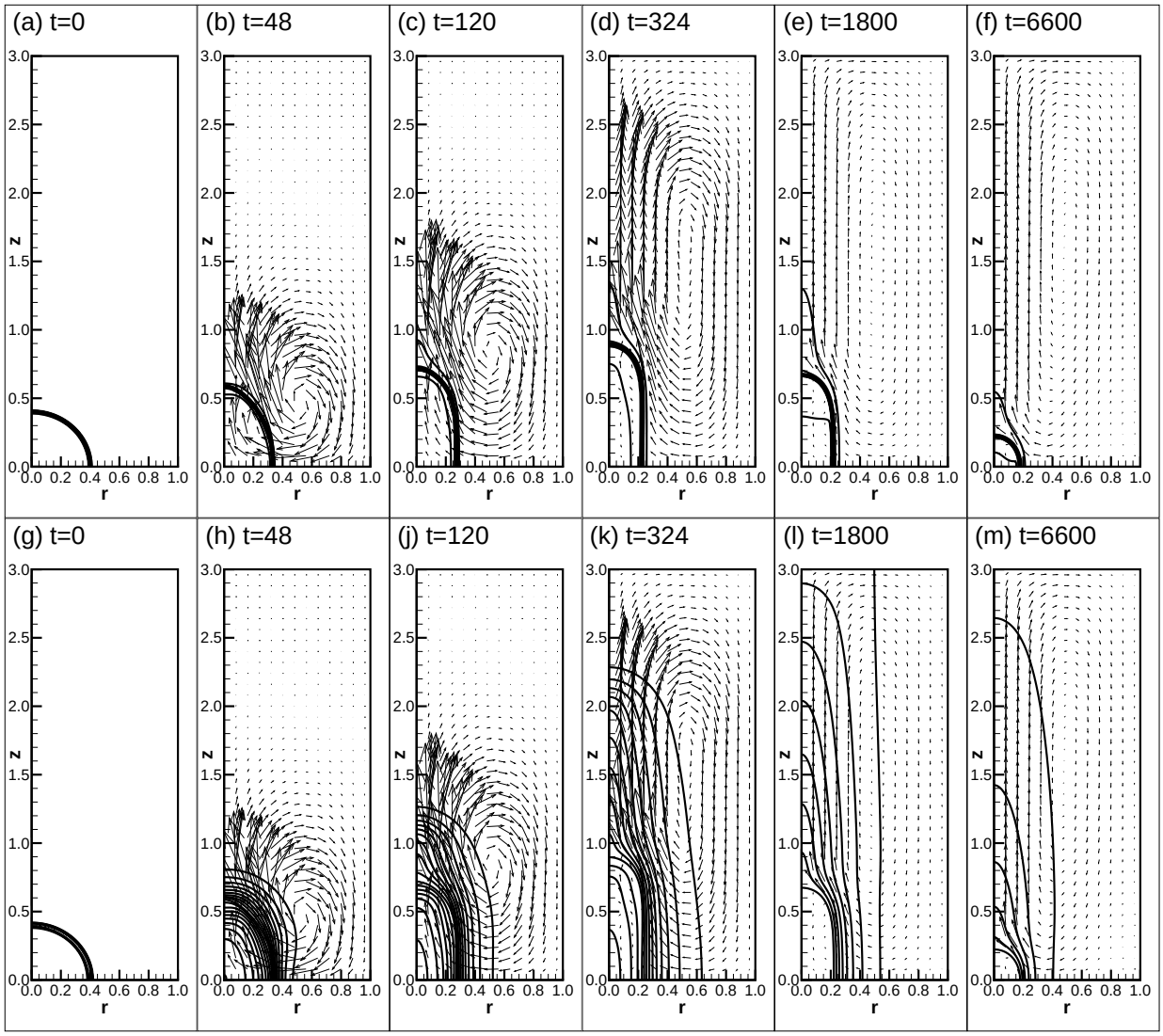

Figure 1: The snapshots of the fields of concentration, velocity, and chemical potential. The results are obtained for $\mathrm{Re} = 10^3$, $\mathrm{Pe} = 5 \cdot 10^5$, $\mathrm{Ca} = 2.5 \cdot 10^{-5}$, $A = -0.5$, $H = 3$, $\mathrm{Gr} = 0.1$ and $r_0 = 0.4$. The upper row shows the fields of concentration and velocity and the lower row shows the fields of chemical potential and velocity. The time moments are indicated in the figure.

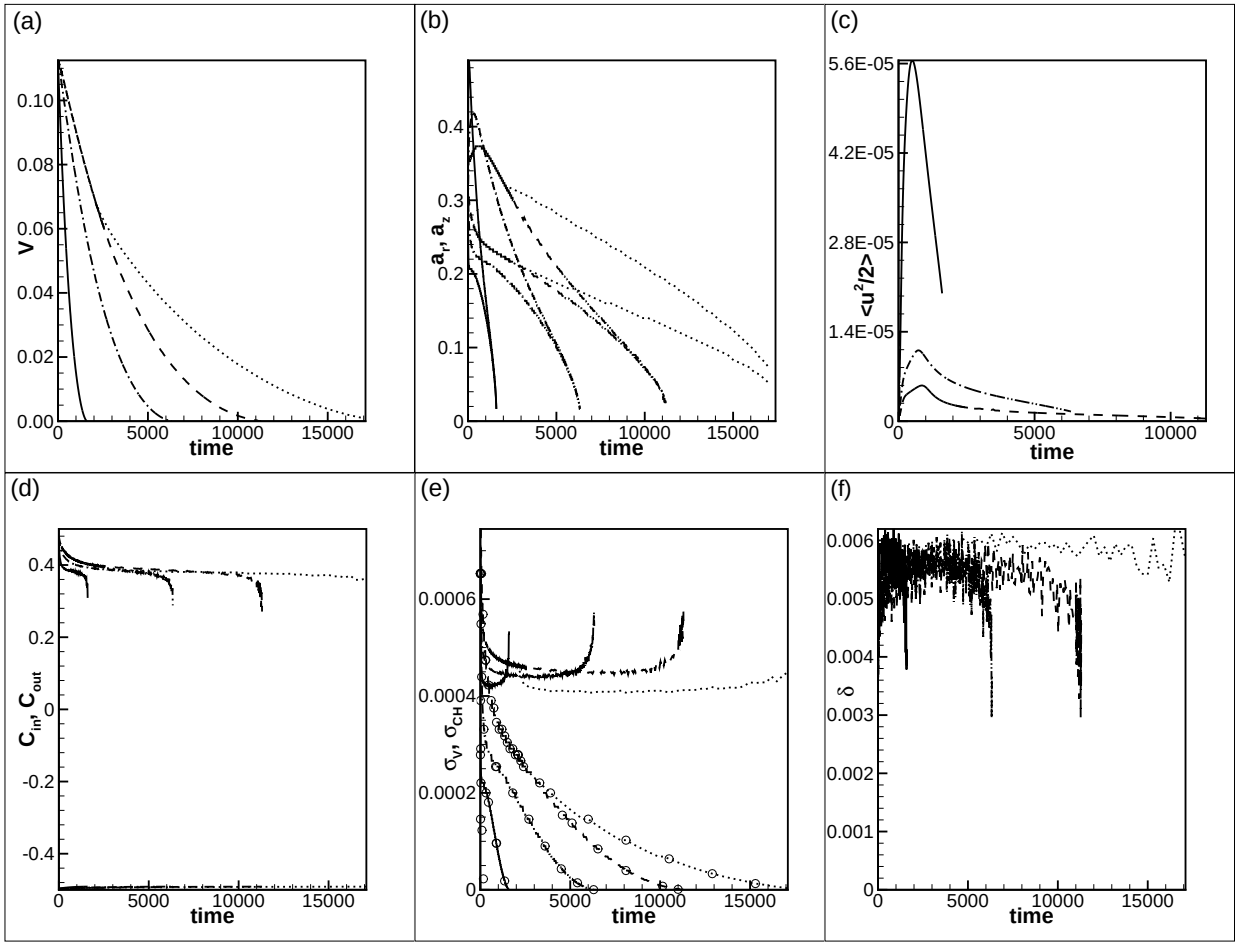

Figure 2: The droplet evolution at different Peclet numbers. The results are shown for $A = -0.5$, $H = 3$, $r_0 = 0.3$, Gr $= 0.1$, Ca $= 2.5 \cdot 10^{-5}$, Re $= 10^3$, and Pe $= 10^5$ (solid line), Pe $= 5 \cdot 10^5$ (dash-dot line), Pe $= 10^6$ (dashed line). The dotted lines are obtained for the run with neglected convective flows (for Pe $= 10^6$). (a) Volume vs. time; (b) droplet's radius and length vs. time; (c) Kinetic energy averaged over the total volume of the tube vs. time; (d) Average concentrations in the droplet and in the surrounding solvent; (e) Surface tension coefficients vs. time, the lines marked by circles depict the curves of the surface tension calculated on the basis of the Vonnegut formula, σ_V, and the other curves show the surface tension coefficients calculated on the basis of the phase-field formula, σ_{CH}; and (f) Interface thickness vs. time.

Pe	$5 \cdot 10^4$	10^5	$5 \cdot 10^5$	10^6
t_f	864	1602	6336	11354

Table 1: The time required for complete dissolution of the droplet, t_f.

different Peclet numbers. Obviously, dissolution occurs slower if the larger values of the Peclet numbers are used. Namely, it was found that the dissolution rate, dV/dt, and the time required for complete dissolution of the droplet are proportional to the Peclet number (see Table 1).

Figure 2 confirms that the time evolution can be split into two stages. The initial short period is characterised by a quick change in the droplet's shape. This change is also accompanied by the stronger hydrodynamic flows. In the end of this stage, the droplet attains an elongated shape that corresponds to a state of quasi-equilibrium. The second stage of the droplet's evolution is characterised by much slower changes of the droplet's shape, and by weaker hydrodynamic motion. The induced hydrodynamic flow is more intensive for the lower values of the Peclet numbers.

The diffusive and hydrodynamic transports are equally important at both stages. The initial stage is primarily driven by hydrodynamics, but the influence of diffusion can be clearly seen from the decay of the droplet's volume. The second stage is primarily driven by the interfacial diffusion, but the contribution of the hydrodynamic flow to the overall mass transport cannot be neglected. To prove the latter statement, a simulation with neglected hydrodynamic terms (but with included barodiffusion) was fulfilled. The run was initiated by an intermediate state that was obtained on the basis of the full program and that was taken within the second stage of the dissolution. The results of the pure diffusive run are depicted in figure 2 by dotted lines. The differences between the run with and without diffusion are particularly seen in terms of the total time needed for complete dissolution. Thus, we conclude that the hydrodynamic flow in the tube substantially increases the dissolution rate.

The average concentration outside the droplet slowly grows by accumulation of the droplet's molecules. The growth remains rather limited owing to small droplet's volume in comparison with the volume of the solute phase. The average concentration in the droplet first experiences a quick drop, approaching the value that corresponds to the thermodynamic equilibrium for the binary mixture (which is 0.388 for a flat interface separating two phases, and if, in addition, all external fields are neglected, and $A = -0.5$). The time of the accommodation of the in-droplet concentration level to the new value is comparable with the time, that is needed for the mechanical transformation of the droplet, that are forced by the changes in the rotation rate (that is the duration of the first stage of the dissolution process). Later, the average concentration within the droplet remains almost constant for the entire process of dissolution.

The values of the surface tension can be determined in two independent ways. The surface tension can be determined from the Vonnegut equation, that was established for immiscible systems, i.e. presuming the balance of the capillary and centrifugal forces and the absence of interfacial diffusion and hydrodynamic flows. In the non-dimensional form, the Vonnegut formula reads,

$$\sigma_{\rm V} = \frac{1}{4}\mathrm{Gr}\, a_r^3. \tag{25}$$

We study the dynamics of miscible droplets, for which only quasi-equilibrium can be established, so that some weak (but non-zero) diffusive and convective mass transfers would always persist. This, in particular, leads to decrease of the droplet's radius, a_r, that is also seen in decrease of the values of the surface tension $\sigma_{\rm V}$ (see figure 2e). At later moments, the droplet becomes nearly spherical, which also makes the Vonnegut formula inapplicable. Nevertheless, a period of slowly-changing values of the surface tension, $\sigma_{\rm V}$, can be noticed, especially, for higher values of the Peclet numbers. In experimental measurements, this period is used for estimations of the surface tension coefficient for miscible liquids.

Another approach is to calculate the value of the surface tension from the structure of the transitional layer that separates the phases (22). The so-calculated surface tension, $\sigma_{\rm CH}$, exhibits a different time-dependence: at the very beginning, the surface tension quickly drops to some value, and then it remains almost constant for the entire duration of the dissolution process, until the very end of the process, when, seemingly, the calculation of the surface tension becomes inaccurate as the thickness of the phase boundary becomes comparable with the size of the droplet itself.

The values $\sigma_{\rm V}$ and $\sigma_{\rm CH}$ are different. It may be argued that the Vonnegut formula can be used just approximately, as no complete balance between the centrifugal and capillary effects is achieved, and which is used to derive the expression for $\sigma_{\rm V}$. The Cahn-Hilliard's surface tension $\sigma_{\rm CH}$ is defined through the properties of the solute/solvent interface that attains the local equilibrium. It should however be also pointed out that at higher Peclet numbers the difference between the val-

ues of the surface tension coefficients becomes smaller. Thus, at very high Peclet numbers, these two values would be even closer.

Finally, the time dependence of the interface thickness is shown in figure 2f. The interfacial thickness was calculated as a ratio between the volume of the transitional zone that separates phases and the droplet's surface area. The transitional zone in turn is defined as the zone with the concentration levels within the range $|C| \leq 1/4$. One sees that the average value of the interface thickness just slightly changes with time and this value is independent of the Peclet number. There are some oscillations about the average value that should be explained by inaccuracies that appear due to low resolution of this smallest length scale: there are about 4 points across the interface, and changes of the interface shape results in slightly different values of the interface thickness.

Figure 3 depicts the results obtained from the simulations performed with different values of the Reynolds number. At the lower Reynolds numbers, the initial droplet's transformations occur slightly slower. The stronger effect is that the attained quasi-equilibrium shapes are different, so the droplet's shape is more elongated at the lower Reynolds numbers. The flows at the lower Reynolds numbers are obviously weaker, but still if these flows are neglected even at the later stage, when all initial transformations of the droplet's shape are completed, the droplet's evolution would occur differently, which is illustrated by the dotted lines.

Figure 4 shows the evolutions of the droplet under different rotation rates (different Grashof numbers). Obviously, an increase in the rate of rotation makes the flows around the droplet more intensive, leading to faster dissolution of the droplet. The coefficients of the surface tension, both σ_{v} and σ_{CH}, and the interface thickness are almost independent of the value of the Grashof number. The rotation rate defines the quasi-equilibrium shape of the droplet: at higher Grashof numbers, the droplet is much stronger elongated, as it should be expected.

Figure 5 depicts the results obtained for the droplets with different initial sizes. It can be shown that the dissolution rate is proportional to the surface area of the droplet, $dV/dt \sim S$. Initially, the droplet dissolves faster, and when the droplet becomes smaller, the rate of the change of its size slows down.

The quasi-equilibrium values of the droplet's radius are almost the same for the droplets of different sizes, but the droplet's length is larger for larger droplets. This is obviously explained by the fact that the surface tension force, that makes the droplet more spherical, is more important for smaller droplets. The values of the surface tension coefficients are almost the same for the droplets of different sizes.

It is useful also to notice that the period when the radius of the droplet remains almost constant (though the length of the droplet is never constant) is much longer for larger droplets. For such droplets, the measurements of the surface tension performed on the basis of the Vonnegut formula would be more accurate.

Figure 6 depicts the results obtained for three different capillary numbers. The values of the surface tension coefficient calculated from the phase-field formula and the values of the interface thicknesses are proportional to $\sqrt{\mathrm{Ca}}$, as expected. The surface tension coefficients calculated from the Vonnegut formula do not change so strongly with the change in the capillary number. There is a capillary number when the values σ_{CH} and σ_{v} would coincide. For our calculations, this would happen for $\mathrm{Ca} \approx 10^{-5}$. For very diffusive interfaces (at higher capillary numbers), the stronger differences from the simple Vonnegut theory should be expected, which is confirmed by our simulations.

At greater capillary numbers (at $\mathrm{Ca} = 4 \cdot 10^{-4}$ for the droplet with initial size $r_0 = 0.3$ and even at $\mathrm{Ca} = 10^{-4}$ for the droplet with initial size $r_0 = 0.4$), during the first stage, that initiated by the abrupt change of the rotation rate, the droplet's shape experiences oscillations with a large amplitude, which are seen in figure 6. These oscillations however die out after several periods.

4. Discussion

The time evolution of an immiscible droplet within a spinning droplet tensiometer was numerically modelled by Hu & Joseph [24], whose main result was the expression for the time changes of the droplet's radius caused by the change of the equilibrium conditions,

$$a_r = a_{r,eq} + (r_0 - a_{r,eq})e^{-mt}, \tag{26}$$

$$m = m_0 \frac{\sigma \mathrm{Re}}{a_{r,eq}} = m_0 \left(\frac{\mathrm{Gr}}{4}\right)^{1/3} \sigma^{2/3} \mathrm{Re}. \tag{27}$$

Here $a_{r,eq}$ is the equilibrium radius of the droplet, and $m_0 = 8.59 \cdot 10^{-3}$. This formula fits the numerical data obtained by Hu & Joseph [24], though they say that comparison of the numerical data with the experimental data was not possible because 'in all of the experiments only limited information was recorded'.

Formula (26) predicts the duration of the first stage of the droplet's evolution. For our typical run, $m \sim 10^{-2}$, and the time of the initial droplet transformation should

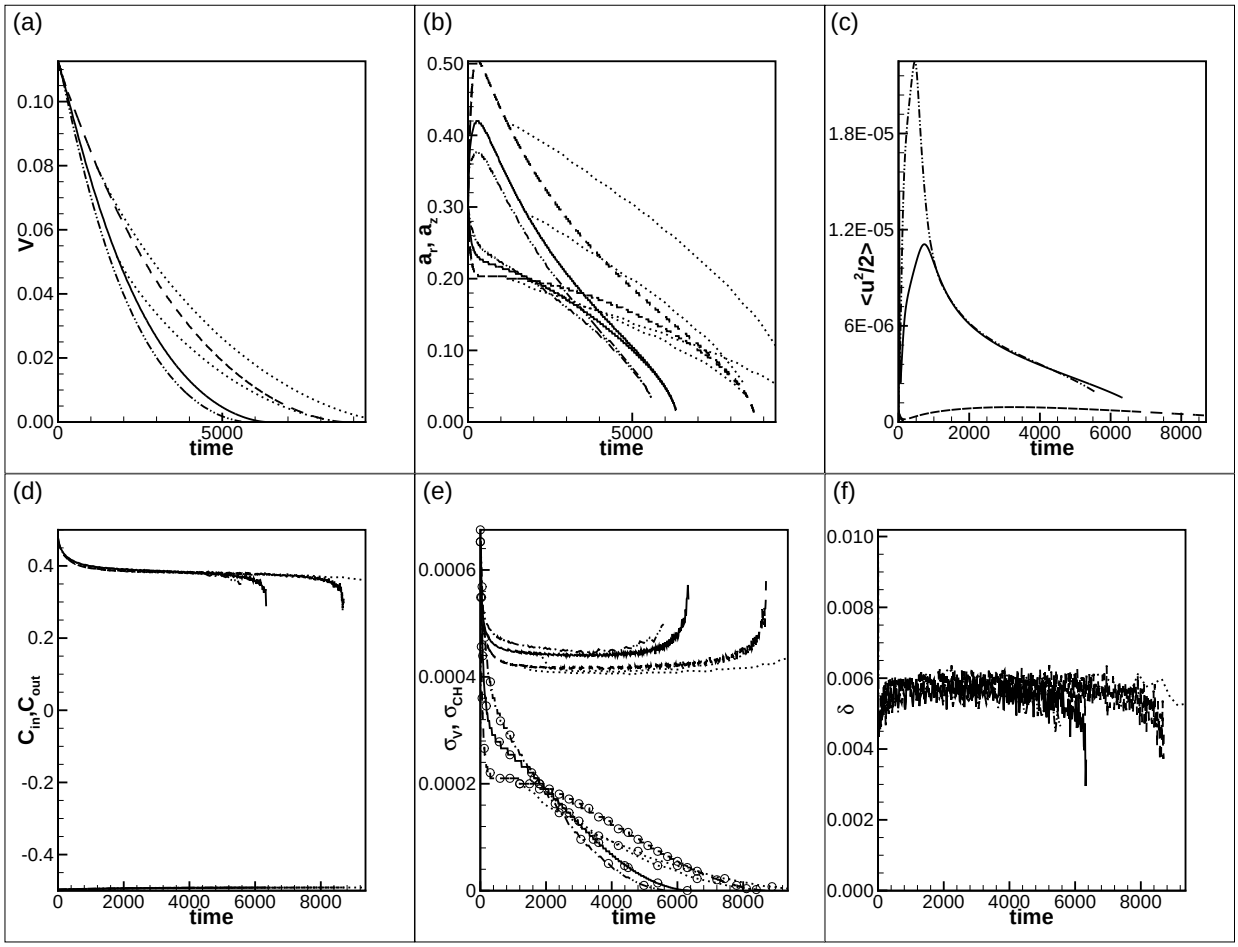

Figure 3: The droplet evolution at different Reynolds numbers. The results are shown for $A = -0.5$, $H = 3$, $r_0 = 0.3$, Gr $= 0.1$, Ca $= 2.5 \cdot 10^{-5}$, Pe $= 5 \cdot 10^5$, and Re $= 100$ (dashed line), Re $= 1000$ (solid line), and Re $= 2000$ (dash-dot line). The dotted lines are obtained for the runs with neglected convective flows. The order of the graphs is as in figure 2.

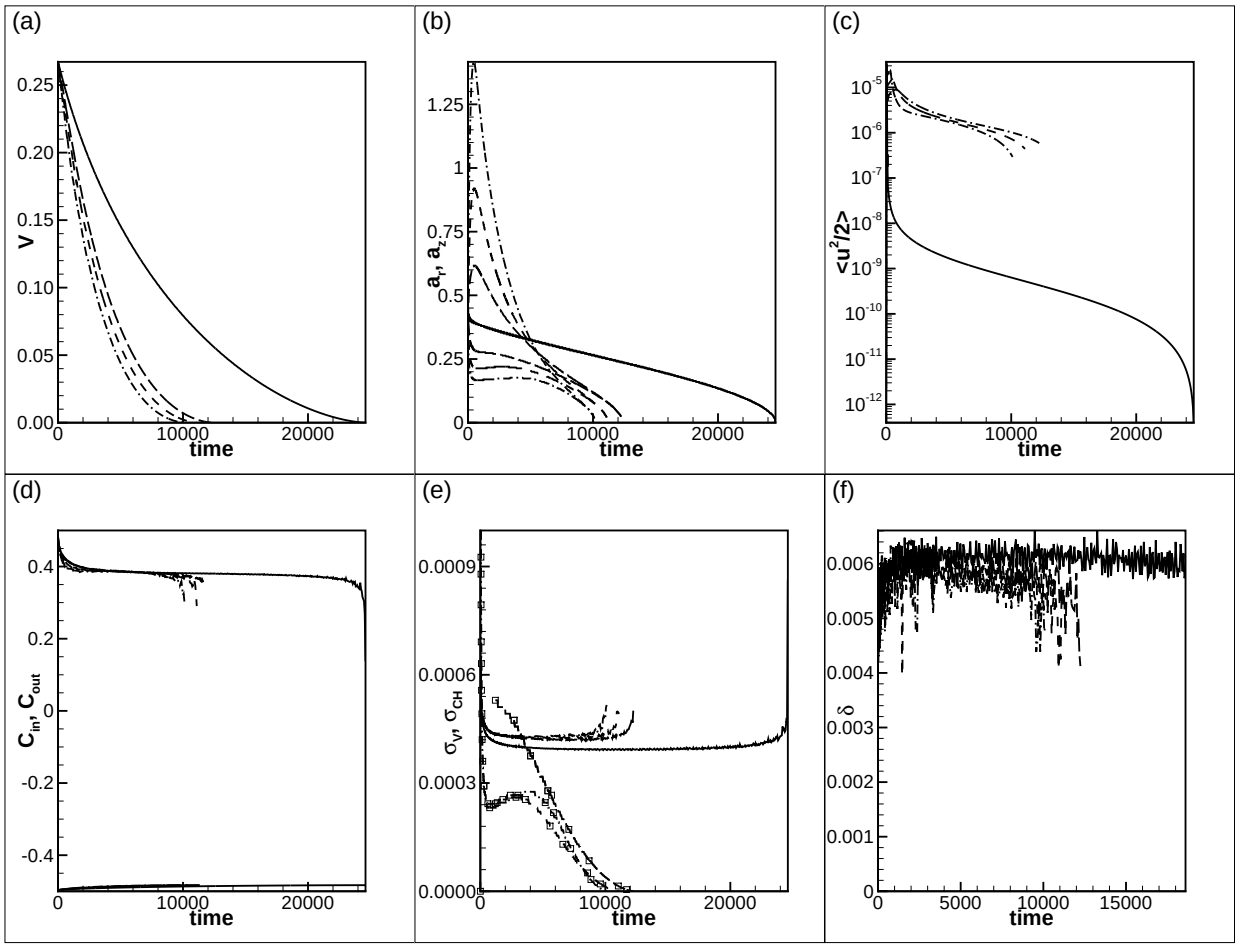

Figure 4: The droplet evolution at different Grashof numbers. The results are shown for $A = -0.5$, $H = 3$, $r_0 = 0.4$, $\mathrm{Ca} = 2.5 \cdot 10^{-5}$, $\mathrm{Pe} = 5 \cdot 10^5$, $\mathrm{Re} = 1000$, and $\mathrm{Gr} = 0$ (solid line), $\mathrm{Gr} = 0.1$ (dashed line), and $\mathrm{Gr} = 0.2$ (dash-dot line). The order of the graphs is as in figure 2.

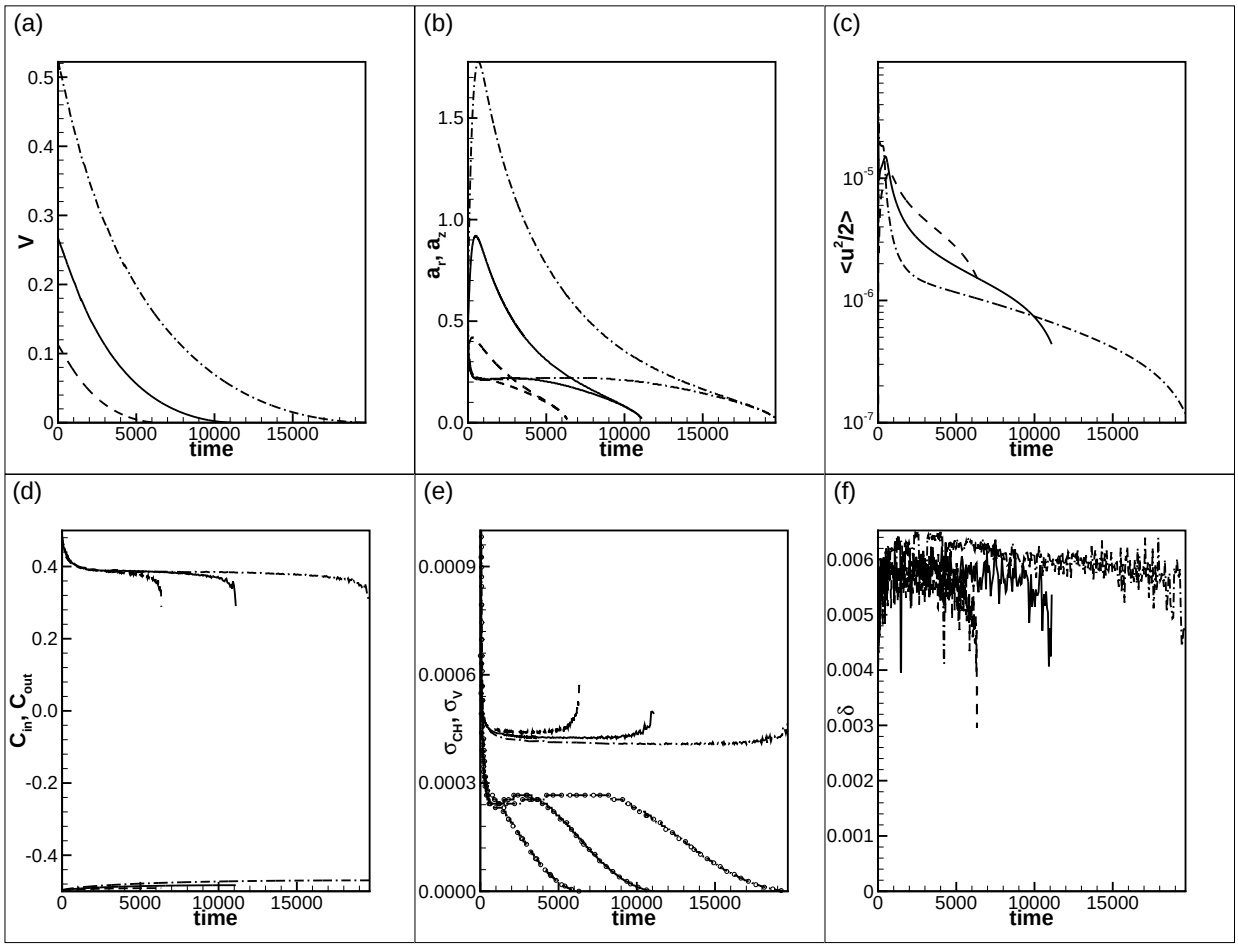

Figure 5: Time evolutions of the droplets of different sizes. The results are shown for $A = -0.5$, $H = 3$, Ca $= 2.5 \cdot 10^{-5}$, Pe $= 10^5$, Re $= 1000$, Gr $= 0.1$, and $r_0 = 0.3$ (solid line), $r_0 = 0.4$ (dashed line), and $r_0 = 0.5$ (dash-dot line). The order of the graphs is as in figure 2.

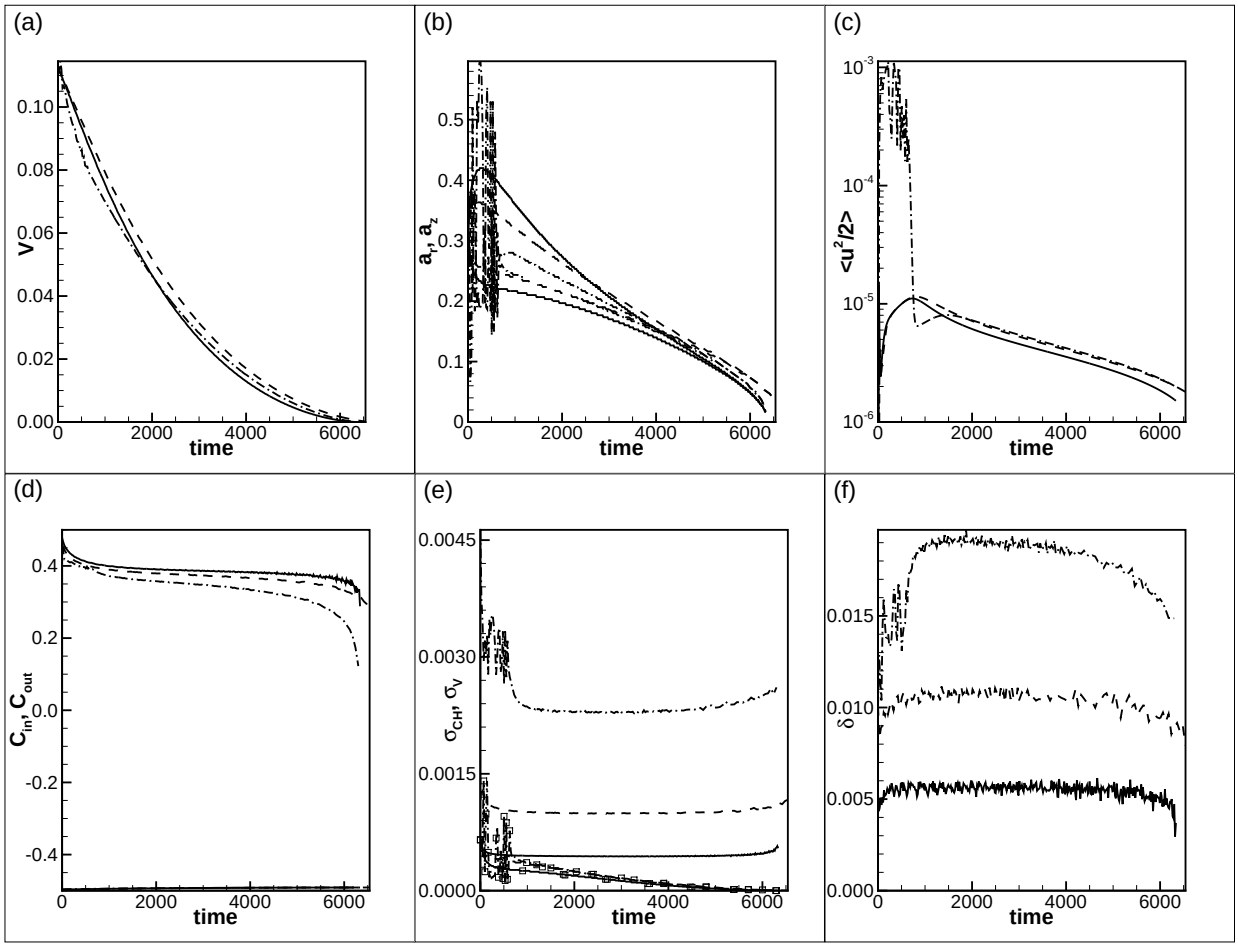

Figure 6: The droplet's evolution calculated for different capillary numbers. The results are shown for $A = -0.5$, $H = 3$, $r_0 = 0.3$, $\mathrm{Pe} = 5 \cdot 10^5$, $\mathrm{Re} = 1000$, $\mathrm{Gr} = 0.1$, and $\mathrm{Ca} = 2.5 \cdot 10^{-5}$ (solid line), $\mathrm{Ca} = 10^{-4}$ (dashed line), and $\mathrm{Ca} = 4 \cdot 10^{-4}$ (dash-dot line). The order of the graphs is as in figure 2.

be of several units of $1/m \sim 100$, which in general agrees well with the presented data.

The dynamics of the miscible droplet was experimentally studied by Heinrich and Wolf [22] and Pojman et al. [19, 20] for the mixtures of isobutyric acid-water and 1-butanol-water, and different polymer solutions. Similar to out observations, it was noted that diffusion was never negligible, and, for instance, the droplet's volume decreases by half within 15 minutes. The non-negligible diffusion makes the measurements of the surface tension at least inaccurate, but, anyway, it was observed that the droplet takes the elongated shape, and the shape can be changed by the change in the speed of the tube's rotation. When the droplet becomes too small, it assumes a nearly spherical shape. The cloudy zones are formed near the droplet's ends. All these experimental observations can be seen in the numerical results reported in this work. Thus, at least, qualitatively, the phase-field approach is capable of accurate reproduction of the dynamics exhibited by the mixtures of two slowly miscible liquids.

The second objective of the current work is to estimate the parameters that are introduced within the phase-field approach. These are the capillary constant, ϵ, the scale for the chemical potential, μ_*, and the coefficient of mobility, α. Currently, the values of these parameters are not known for any particular mixture of liquids. Even their typical orders are not known. This significantly hinders wider usage of the phase-field approach. The values of these parameters can though be derived through the comparison of the numerical results reported in this work with the experimental data available for the spinning droplet tensiometer.

In the experiments, the measurements of the surface tension coefficients using the spinning drop tensiometer are based on the Vonnegut's formula (1). The interfacial mass transfer is never negligible in the experiments and in our results, which renders the measured values inaccurate. Nevertheless, in the experiment [19], the typical order of the surface tension coefficient for a pair of two miscible liquids is given as $\sigma \sim 10^{-5} N/m$. From our data one sees that the typical order of the surface tension coefficient is $\sigma_{\text{V}} \sim 10^{-4}$. Between these two quantities, there is the following relationship, $\sigma = \rho_* \mu_* L_* \sigma_{\text{V}}$ ($\rho_* \mu_* L_*$ is the unit of the surface tension). Thus, if the tensiometer's tube has the radius, $R = L_* \sim 10^{-3} m$, and the mixing of liquids is characterised by the typical density, $\rho_* \sim 10^3 kg \cdot m^{-3}$, one obtains that the typical value of the chemical potential is $\mu_* \sim 0.1\ J \cdot kg^{-1}$.

The surface tension coefficients, σ_{V} and σ_{CH}, are different in all calculations reported. The surface tension coefficient, σ_{CH}, is determined by the value of the capillary number, and at some capillary number, $\sim 10^{-5}$, these two coefficients would have nearly same values (as can be seen in figure 6).

The numeric value of the surface tension coefficient, σ_{CH}, can be approximately calculated from the formula for a flat interface $\sigma_0 = \frac{\sqrt{Ca}}{6\sqrt{2}} \sim 10^{-1} \sqrt{\frac{\epsilon}{\mu_* L_*^2}}$, which allows us to conclude that the typical value of the capillary constant is $\epsilon \sim 10^{-13}\ m^4 \cdot s^{-2}$. Previously, the value of the capillary constant was estimated as $10^{-18}\, m^4 \cdot s^{-2}$ for a honey-water mixture [29] and $(10^{-16} - 10^{-14})\, m^4 \cdot s^{-2}$ for a monomer/polymer solution [20, 30].[5]

Finally, in the experiments (e.g. [19]), the time period needed for complete dissolution of the droplet with the initial radius $\sim 0.5R$ is of the order of $10^4 s$. The accepted time scale, $\tau = \frac{R}{\mu_*^{1/2}} \sim 10^{-3} s$, and thus the typical non-dimensional time needed for dissolution of the droplet is $t_f \sim 10^7$. From our calculations (using figures 2 and 4), one concludes that such a time would characterise the numerical calculation done with $Pe \sim 10^9$. Using the definition of the Peclet number (10), one concludes that the mobility coefficient is of the order, $\alpha \sim 10^{-9}\ kg \cdot s \cdot m^{-3}$.

Let us now use these values to determine the 'right' orders of the non-dimensional parameters. As already mentioned, the 'right' value of the capillary number is 10^{-5}. This, for instance, gives the typical thickness of the phase boundary (as a good estimate, the formula for a flat interface can be used, i.e. $\delta = \sqrt{-\text{Ca}/A}$) as $10^{-6} m$. This estimate agrees with the experimental measurements [20].

The Reynolds number is $\text{Re} \sim 10^3$, and the Grashof number is $\text{Gr} \sim 10^{-3}$. For the latter estimations, the following typical viscosity, $\eta_* \sim 10^{-3} Pa \cdot s$, the density contrast, $\phi \sim 10^{-2}$, and the rotation rate $\sim 100 rps$ were used.

The results presented in this paper are given for the lower values of the Peclet number, as the calculations for the higher Peclet numbers become computationally too demanding. Nevertheless, we found that both the rate of dissolution and the total time needed for dissolution are proportional to the Peclet number. There are also no qualitative changes in the droplet's behaviour upon increase of the Peclet number. These observations permit us to draw the conclusions about the behaviour of the real droplet from the obtained data. We have also presented most of the data for the Grashof number $Gr = 0.1$, which is higher than the estimate 10^{-3}

[5] In the referenced works [29, 20, 30], the capillary constant is $(\rho_* \epsilon)$ and is measured in N. The reported values are re-calculated in accordance with the definitions accepted in this work.

(or 10^{-2} for the higher rates rotation). The higher value was used to demonstrate the elongation of the droplet. Most of the results are reported for the smaller droplet than in the experiments (where it is typically, $r_0 \sim 0.5$), and for larger droplet the droplet would be sufficiently elongated for smaller values of the Grashof number.

We would like also to note that the estimations for the values of the non-dimensional parameters agree with the other numerical works, e.g. [25], where the ratio $\delta_{CL} \equiv \mathrm{Ca}/(16\mathrm{Gr})$ is set for the calculations. In [25], a better agreement with the experimental data is achieved at $\delta_{CL} \sim 10^{-5} - 10^{-6}$, which would correspond to $\mathrm{Ca} \sim 10^{-5} - 10^{-6}$ and $\mathrm{Gr} \sim 10^{-1} - 10^{-2}$.

5. Conclusions

In this work, it is shown that the phase-field approach correctly describes the behaviour of two slowly miscible liquids within the spinning droplet tensiometer, both at the short and long time scales. The approach correctly predicts the evolution of the shape of the droplet, predicting such experimentally-observed details of the process as the existence of the sharp phase boundary for the entire dissolution, non-negligible interfacial mass transfer during any stage of the process including the initial stage after the change the rotation speed when the droplet quickly accommodates to the new shape, the cloudy regions near the droplet's ends, the independence of interfacial stresses on the speed of the tube's rotation and the size of the immersed droplet, and some others [22, 19, 20]. This also confirms our earlier phase-field-based calculations fulfilled for the mixture of miscible liquids within a different geometry [39].

Another achievement of the current work is the estimation of the phenomenological parameters introduced within the phase-field approach. The use of the non-standard parameters is the significant drawback of the approach, which significantly slows down the wider acceptance of the approach. It is still difficult to obtain these parameters accurately, since the current computational capabilities do not allow us to run the simulations for the realistic values of all parameters that would permit the full correspondence between the experimental pictures and the numerical results. Nevertheless, extrapolation of the computational results allows us to estimate the 'right' values of the parameters for which such a correspondence can be achieved. In particular, it is found that the 'right' order of the scale for the chemical potential is $0.1\ J \cdot kg^{-1}$, the 'right' order of the capillary constant is $10^{-13}\, m^4 \cdot s^{-2}$, and the 'right' order of the mobility coefficient is $10^{-9} kg \cdot s \cdot m^{-3}$. The knowledge of these parameters would permit meaningful calculations to be fulfilled on the basis of the phase-field approach for tracing the evolution of miscible liquids within other geometries. This necessary step has never been done. Only the capillary constant was previously estimated [20, 30], and the previous estimations are close to the value obtained in the current work.

6. Appendix. Symbol list

$\bar{C}$; C_{cr}; $C = \bar{C} - C_{cr}$	concentration; value of concentration at the critical point; concentration with shifted reference point;
$\bar{\rho}$; ρ_{cr}; $\rho = \bar{\rho} - \rho_{cr}$;	density; density at the critical point; density with shifted reference point;
ρ_1 and ρ_2; ϕ	densities of pure solvent and solute; density contrast (2);
f; f_0	specific free energy; classical part of the specific free energy (3);
ϵ	capillary constant (3);
μ; μ_0	chemical potential; classical part of the chemical potential;
a and b	phenomenological parameters determining the thermodynamic state of a mixture;
α	mobility constant;
Ω	angular velocity of the tube's rotation;
R; H	radius of the tube; half-length of the tube scaled in unites of R;
a_r; a_z; r_0; $a_{r,eq}$	non-dimensional radial and axial dimensions of the droplet (measured in units of R); radius of an initial (spherical) droplet; droplet's radial dimension in the equilibrium state (for an immiscible droplet)
C_0; C_{in}	equilibrium concentration profile for a flat interface (21); initial concentration profile (24);
δ; δ_0; δ_{in}	interface thickness; thickness of an equilibrium flat interface (21); initial thickness of an interface;
r and z; $\vec{e}_r$	radial and axial coordinates; the unit vector in the radial direction;
$\vec{u} = (u_r, u_z)$	vector of velocity;
Π	pressure field;
ω and ψ	vorticity and streamfunction (20);
L_*; τ_*; v_*; p_*; μ_*	typical length and time, velocity, pressure and chemical potential (9);
Pe; Ca; Re; Gr	Peclet (10), capillary (11), Reynolds (12), and Grashof (13) numbers;
A	non-dimensional parameter determining the thermodynamic state of a mixture
σ; σ_0; σ_v; σ_{CH}	surface tension coefficient; surface tension coefficient for a flat interface (23); surface tension coefficient calculated from the Vonnegut formula (25); surface tension coefficient calculated from the structure of the solute/solvent interface (22);
m; m_0	rate of change of the droplet's radial dimension; a constant (26)

7. Acknowledgments

The work was supported by Russian Science Foundation (Grant No. 14-21-00090).

[1] B. Vonnegut, Rotating bubble method for the determination of surface and interfacial tensions, Rev. Sci. Instrum. 13 (6) (1942) 6–9.

[2] T. R. Fink, D. P. Hearn, Multicell spinning drop interfacial tensiometer, Rev. Sci. Instrum. 49 (2) (1978) 188–193.

[3] Y. Seeto, L. E. Scriven, Precision spinning drop interfacial tensiometer, Rev. Sci. Instrum. 53 (11) (1982) 1757–1761.

[4] H. M. Princen, I. Y. Z. Zia, S. G. Mason, Measurement of interfacial tension from the shape of a rotating drop, Journal of Colloid and Interface Science 23 (6) (1967) 99–107.

[5] C. D. Manning, L. E. Scriven, On interfacial tension measurement with a spinning drop in gyrostatic equilibrium, Rev. Sci. Instrum. 48 (12) (1977) 1699–1705.

[6] P. K. Currie, J. V. Nieuwkoop, Buoyancy effects in the spinning-drop interfacial tensiometer, Journal of Colloid and Interface Science 87 (2) (1982) 301–316.

[7] H. M. Princen, Some aspects of spinning drop apparatus, Journal of Colloid and Interface Science 169 (1) (1995) 241–243.

[8] H. M. Princen, R. Vaidya, Shape of menisci in spinning horizontal tubes: Application to contact angle determination, Journal of Colloid and Interface Science 174 (1) (1995) 68–78.

[9] L. C. Levy, W. R. McGillisy, J. T. Germaine, P. J. Culligan, Spinning drop tensiometry using a square section sample tube, Journal of Colloid and Interface Science 234 (2) (2001) 442–444.

[10] C. C. V. Chan, J. A. W. Elliott, M. C. Williams, Investigation of the dependence of inferred interfacial tension on rotation rate in a spinning drop tensiometer, Journal of Colloid and Interface Science 260 (1) (2003) 211–218.

[11] A. Vorobev, Dissolution dynamics of miscible liquid/liquid interfaces, Current Opinion in Colloid and Interface Science 19 (2014) 300–308.

[12] D. Korteweg, Sur la forme que prennent les equations du movement des fluides si l'on tient compte des forces capillaires causees par des variations de densite, Arch. Neel. Sci. Ex. Nat. (II) 6 (6) (1901) 1–24.

[13] J. van der Waals, The thermodynamic theory of capillarity under the hypothesis of a continuous variation of density, Vehandel Konink. Acad. Weten. Amsterdam 1 (Sect. 1) (1892) 1–56, translation by J.S. Rowlingson, L. Statist. Phys, 20:1970244, 1979.

[14] Y. B. Zeldovich, About surface tension of a boundary between two mutually soluble liquids, Zhur. Fiz. Khim. 23.

[15] D. Joseph, Fluid dynamics of two miscible liquids with diffusion and density gradient, Eur. J. Mech. B/Fluids 9 (9) (1990) 565–596.

[16] P. Smith, M. V. D. Ven, S. G. Mason, The transient interfacial tension between two miscible fluids, J. Colloid Interface Sci. 80 (1) (1981) 302–303.

[17] S. E. May, J. V. Maher, Capillary-wave relaxation for a meniscus between miscible liquids, Physical Review Letters 67 (1991) 2013–2016.

[18] L. Lacaze, P. Guenoum, D. Beysens, M. Delsanti, P. Petitjeans, P. Kurowski, Transient surface tension in miscible liquids, Physical Review E 82 (2010) 041606.

[19] J. A. Pojman, C. Whitmore, M. L. T. Liveri, R. Lombardo, J. Marszalek, R. Parker, B. Zoltowski, Evidence for the existence of an effective interfacial tension between miscible fluids: Isobutyric acid-water and 1-butanol-water in a spinning-drop tensiometer, Langmuir 22 (6) (2006) 2569–2577.

[20] B. Zoltowski, Y. Chekanov, J. Masere, J. A. Pojman, V. Volpert,

Evidence for the existence of an effective interfacial tension between miscible fluids. 2. dodecyl acrylate-poly(dodecyl acrylate) in a spinning drop tensiometer, Langmuir 23 (10) (2007) 5522–5531.

[21] Y. Gaponenko, M. Torregrosa, V. Yasnou, A. Mialdun, V. Shevtsova, Dynamics of the interface between miscible liquids subjected to horizontal vibration, J. Fluid Mech. 784 (2015) 342–372.

[22] M. Heinrich, B. A. Wolf, Establishment of phase equilibria: Temperature jump experiments in a spinning-drop apparatus, Macromolecules 26 (22) (1993) 6106–6110.

[23] P. Petitjeans, Une tension de surface pour les fluides miscibles, C. R. Acad. Sci. Paris 322 (2b) (1996) 673–679.

[24] H. H. Hu, D. D. Joseph, Evolution of a liquid drop in a spinning drop tensiometer, Journal of Colloid and Interface Science 162 (2) (1994) 331–339.

[25] C. Y. Chen, K. T. Liu, Numerical simulations of a miscible drop in a spinning drop tensiometer, Journal of Mechanics 23 (23) (2007) 1–7.

[26] J. Lowengrub, L. Truskinovsky, Quasi-incompressible cahn-hilliard fluids and topological transitions, Proc. R. Soc. London, Ser. A 454.

[27] A. Vorobev, Boussinesq approximation of the cahn-hilliard-navier-stokes equations, Phys. Rev. E 82 (10) (2010) 056312–056312.

[28] J. Jacqmin, Calculation of two-phase navier-stokes flows using phase-field modelling, J. Comp. Phys. 155 (1999) 96–127.

[29] J. A. Pojman, N. Bessonov, V. Volpert, M. S. Paley, Miscible fluids in microgravity (mfmg): a zero-upmass investigation on the international space station, Microgravity Sci, Technol. XIX-1 (2007) 33–41.

[30] J. A. Pojman, Y. Chekanov, V. Wyatt, N. Bessonov, V. Volpert, Numerical simulations of convection induced by korteweg stresses in a miscible polymer-monomer system: effects of variable transport coefficients, polymerization rate and volume changes, Microgravity Sci. Technol 21.

[31] M. Stevar, A. Vorobev, Shapes and dynamics of miscible liquid/liquid interfaces in horizontal capillary tubes, Journal of Colloid and Interface Science 383 (2012) 184–197.

[32] M. Stevar, A. Vorobev, Dissolution dynamics of liquid/liquid binary mixtures within a micromodel, Transport in Porous Media 100 (2012) 184–197.

[33] J. Cahn, J. Hilliard, Free energy of a nonuniform system. i. interfacial free energy, J. Chem. Phys. 28 (1958) 258–267.

[34] L. D. Landau, E. M. Lifshitz, Statistical Physics, 3rd Edition, Part 1, Pergamon Press, 1980.

[35] H. G. Lee, J. S. Lowengrub, J. Goodman, Modeling pinchoff and reconnection in a hele-shaw cell. i. the models and their calibration, Physics of Fluids 14 (2) (2002) 492–513.

[36] H. G. Lee, J. S. Lowengrub, J. Goodman, Modeling pinchoff and reconnection in a hele-shaw cell. ii. analysis and simulation in the nonlinear regime, Physics of Fluids 14 (2) (2002) 514–545.

[37] A. Kheniene, A. Vorobev, Linear stability analysis of a horizontal phase boundary separating two miscible liquids, Phys. Rev. E 88 (2) (2013) 022404.

[38] A. Kheniene, A. Vorobev, Linear stability of a horizontal phase boundary subjected to shear motion, Eur. Phys. J. E 38 (2015) 77.

[39] R. Xie, A. Vorobev, On the phase-field modelling of a miscible liquid/liquid boundary, Journal of Colloid and Interface Science 264 (2015) 48–58.